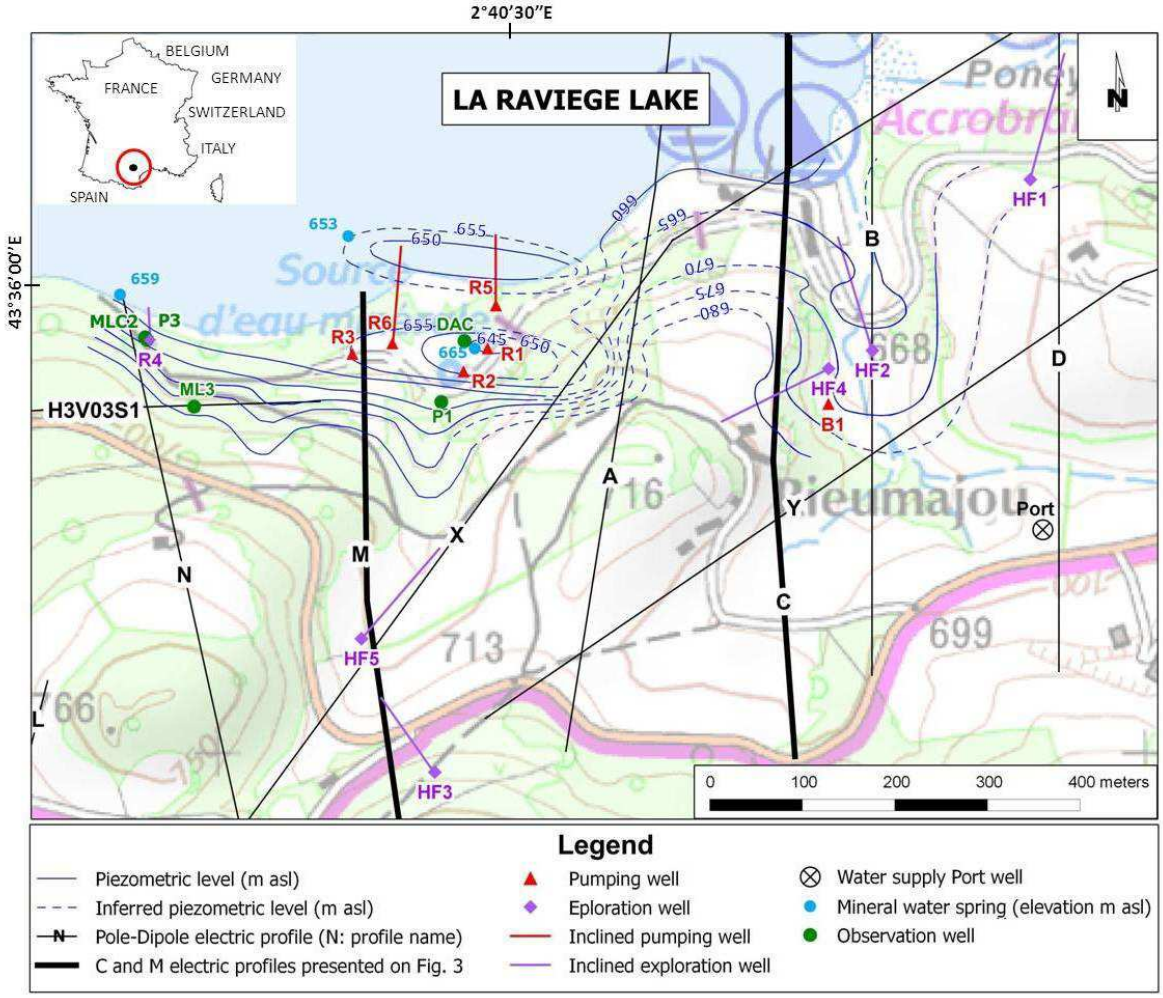

Figure 1: La Salvetat natural mineral waters field in southern France showing the location of the main wells used in this study. Shown also is the piezometric map of the mineral aquifer and the location of pole-dipole electric profiles. The legend of the underlying topographic map is available at http://www.routebuddy.com/routebuddy/routebuddy-manual/useful-links-incl-map-keys/ign-25k-map-key

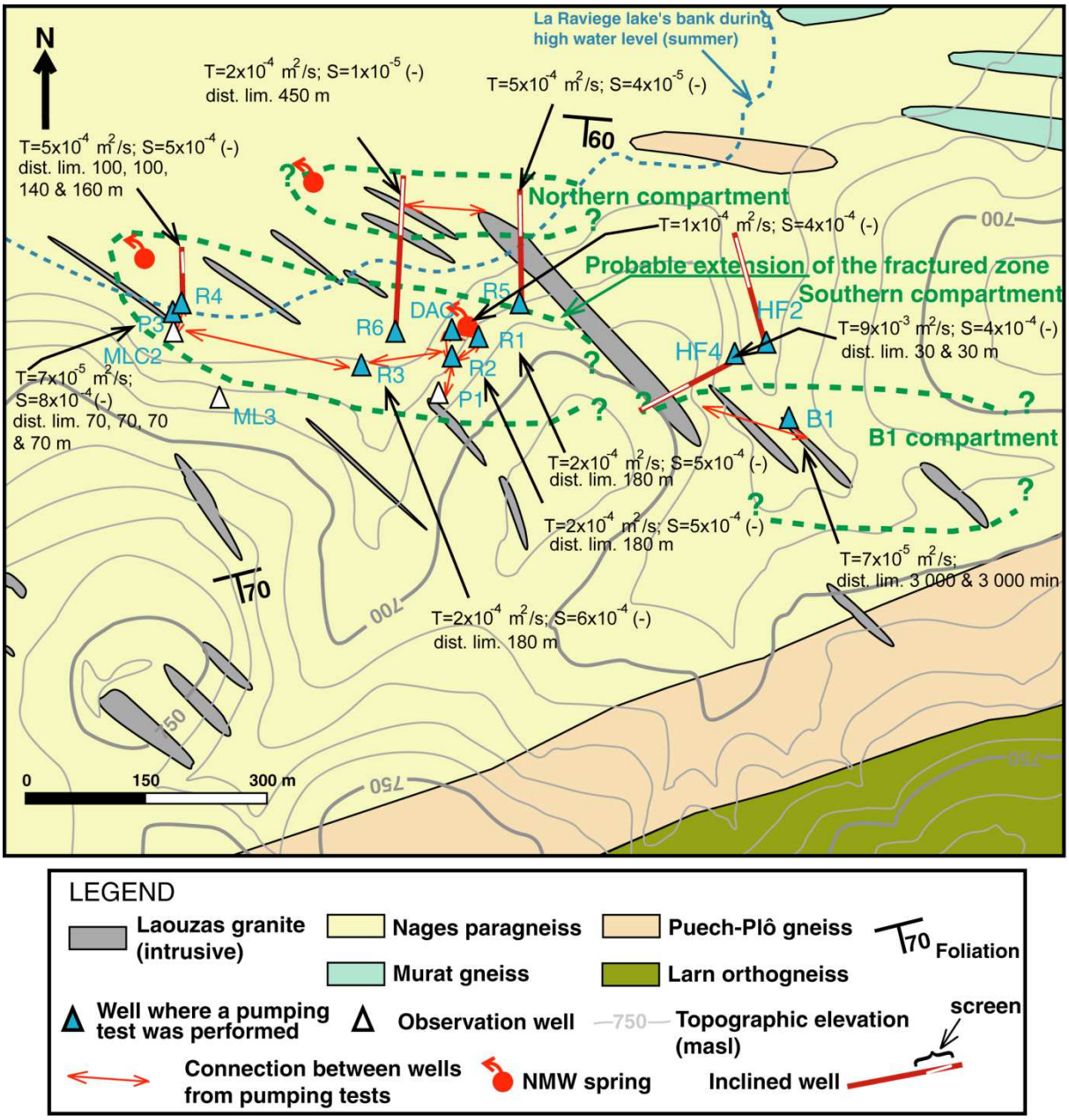

Figure 2: Hydrogeological map of the mineral waters field with pumping test results and probable extension of mineral-water bearing fracture zones (T: transmissivity; S: storativity; dist. lim.: distance from pumping well to no-flow boundaries)

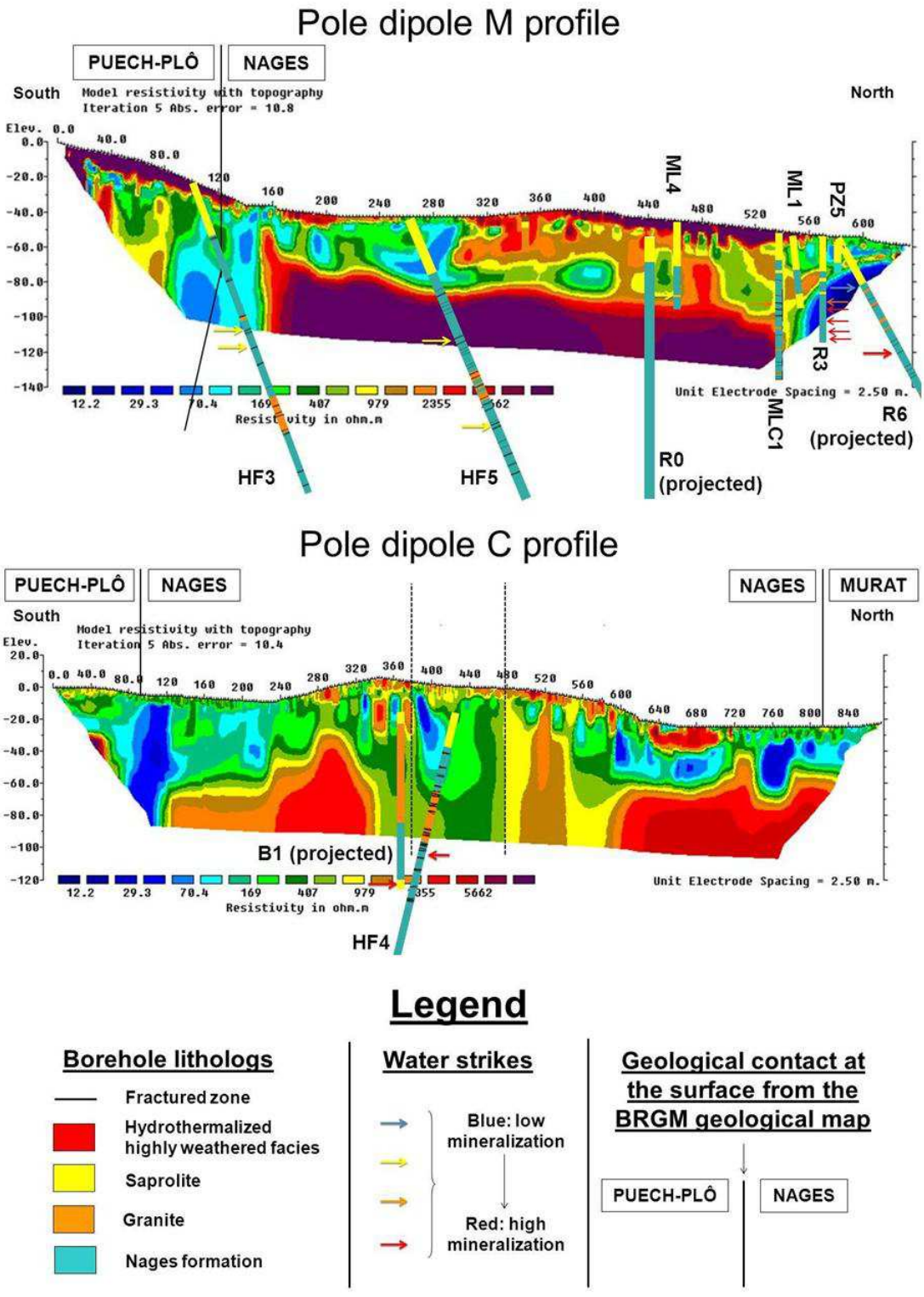

Figure 3 : Results of pole-dipole geophysical north-south profiles M and C

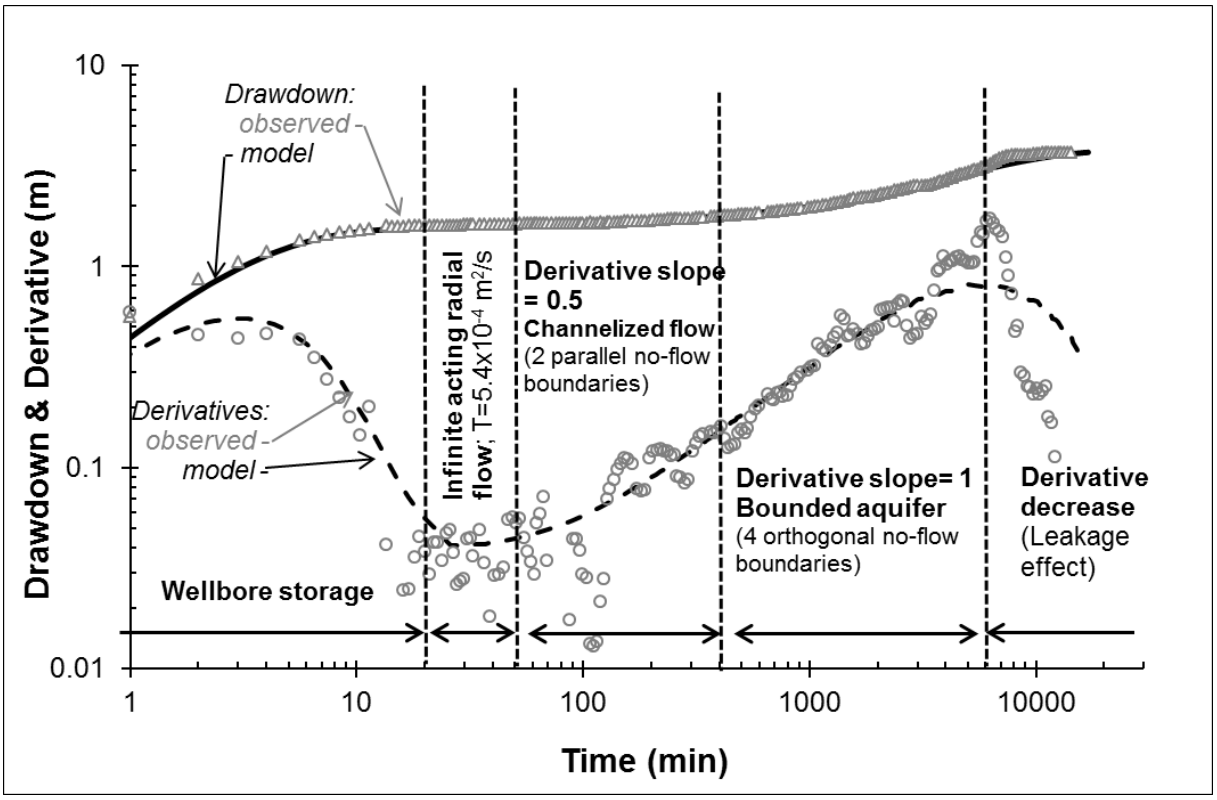

Figure 4: A 10-day pumping test on R4 with its diagnostic curve and modelling using an analytical solution for a rectangular aquifer with leakage effect. Flow rate 9 m^3/h. Model parameters: T: 5.5 x 10^{-4} m^2/s, S: 5 x 10^{-4} (-), rectangular aquifer: 0.09 km^2, transmissivity of the aquitard: 10^{-6} m^2/s.

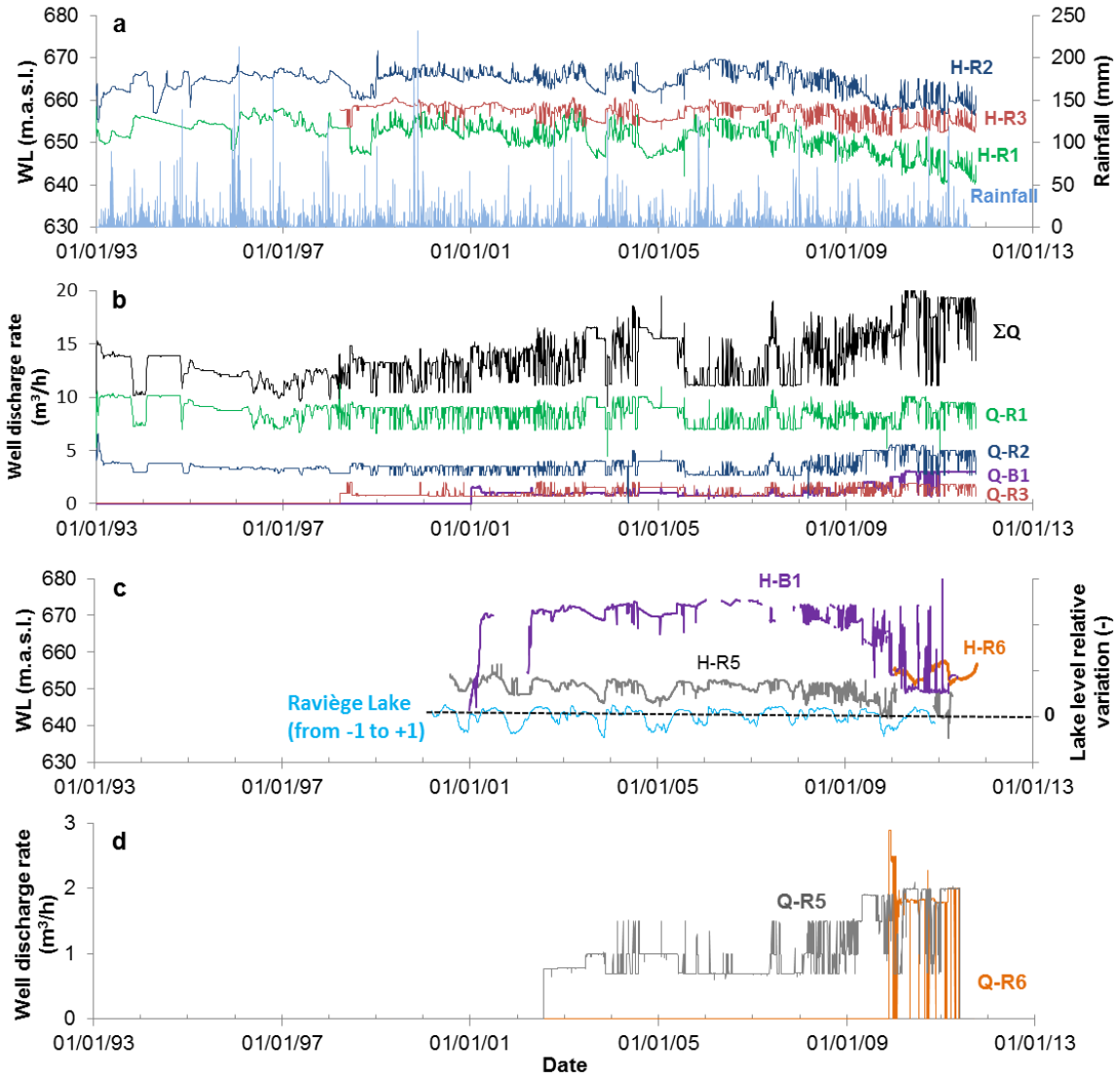

Figure 5 : (a)Water levels in wells R1, R2 and R3 and rainfall time series; (b) discharge rates in wells B1, R1, R2, R3; (c) Raviège Lake level relative variations and water levels in wells B1, R5 and R6; (d) discharge rates in wells R5 and R6. WL: water level; Q: discharge

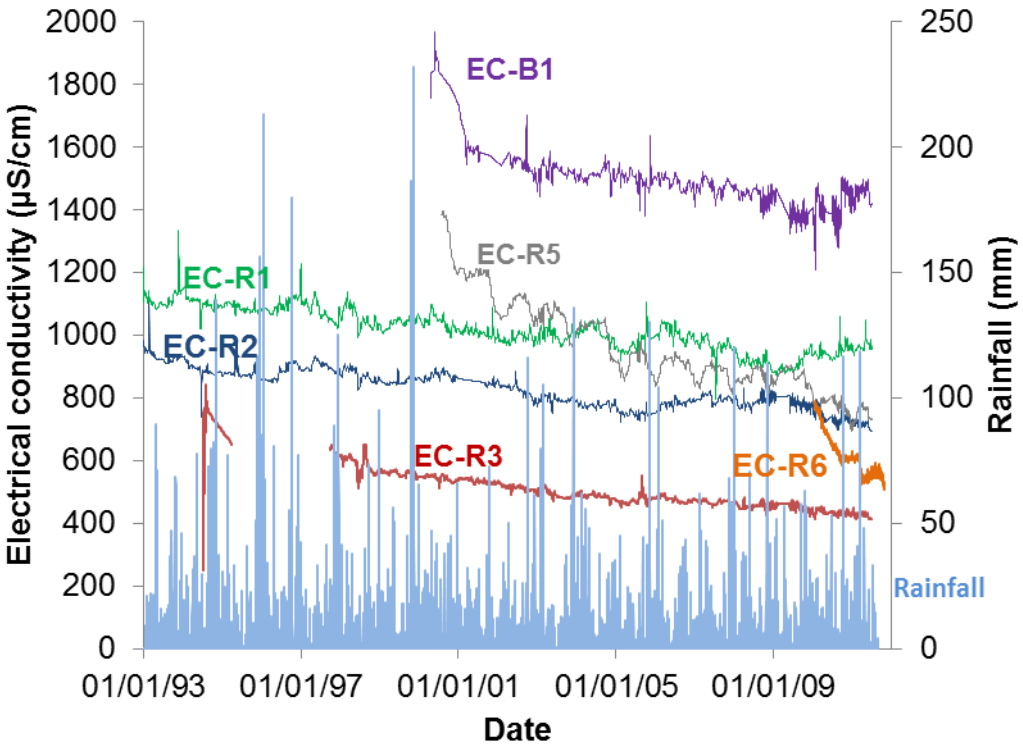

Figure 6 : Electrical conductivity (EC) trends in pumped wells

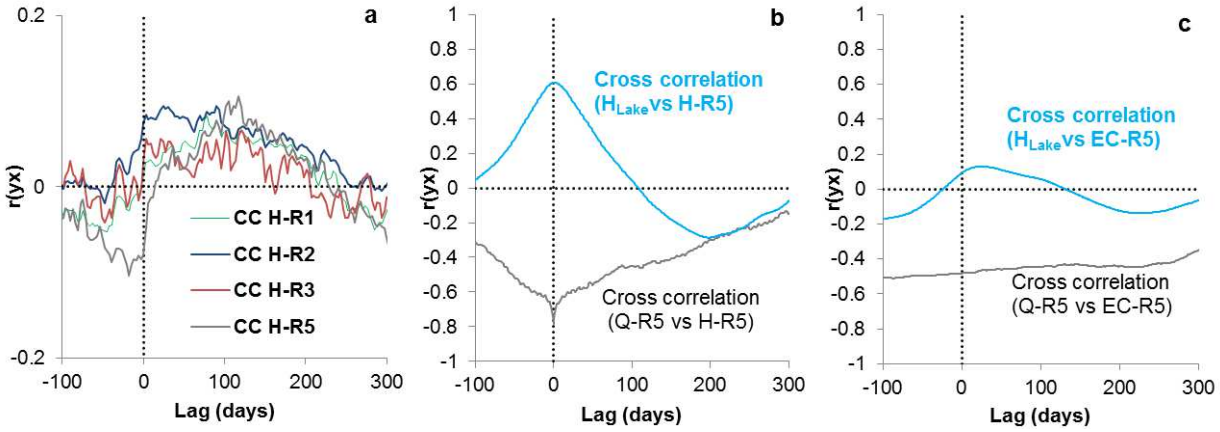

Figure 7: Cross correlation (CC) analysis: (a) between rainfall and water level measurements in wells R1, R2, R3 and R5, (b) between lake level (H) or pumping rate (Q) and water level measured in well R5, and (c) between lake level or pumping rate and EC measured in well R5; r(yx): correlation coefficient

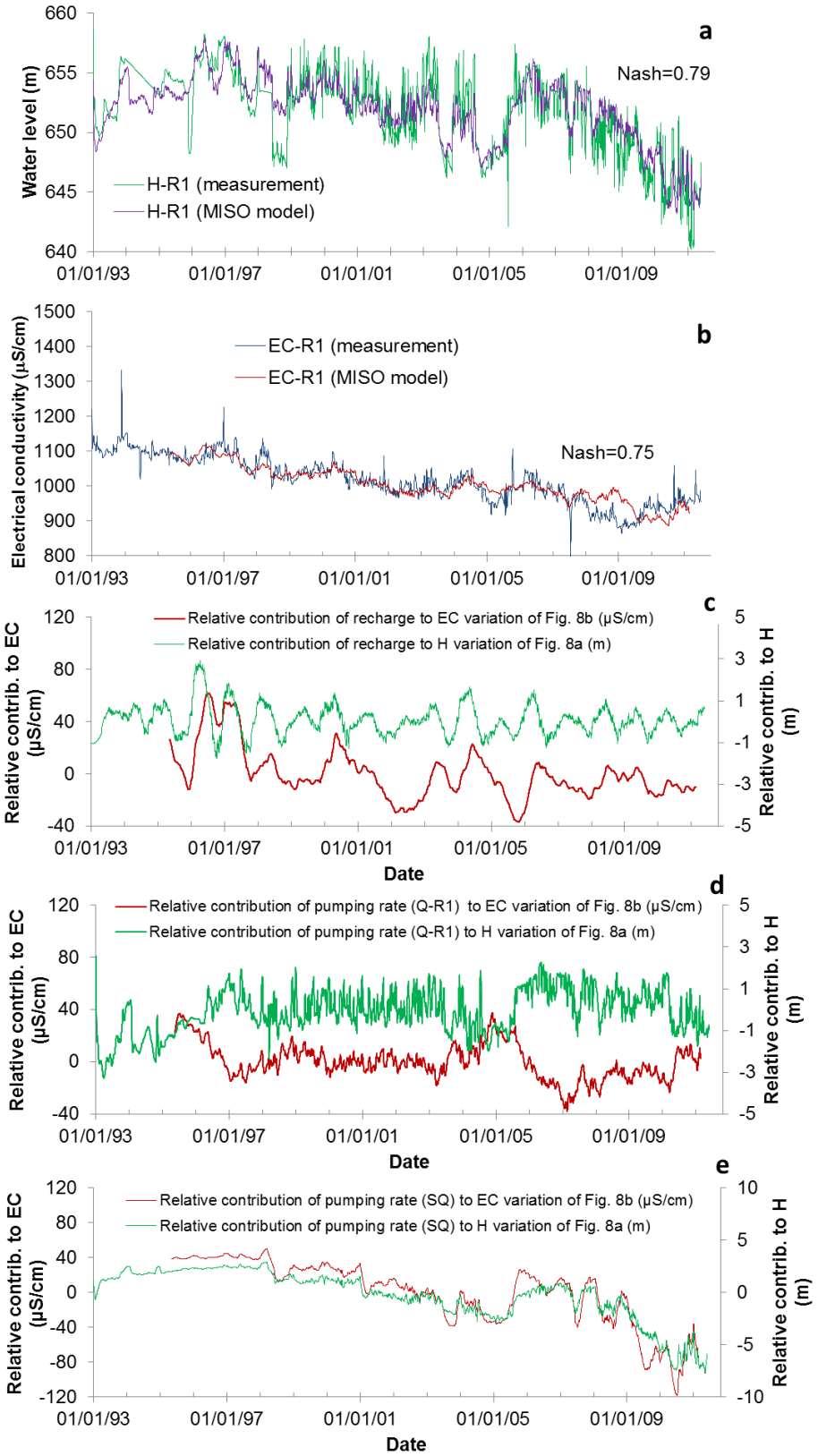

Figure 8: Multiple input single output (MISO)deconvolution results. (a) water levels at R1 – comparison between measurement and MISO model output, (b) electrical conductivity (EC) at R1 – comparison between measurement and MISO model output , (c) relative contributions of rechargeto water level (H) and EC fluctuations at R1 estimated from MISO analysis, (d) relative contributions of pumping rate at R1 to H and EC fluctuations estimated from MISO analysis, (e) relative contributions of total pumping rate at R1 to H and EC fluctuations estimated from MISO analysis

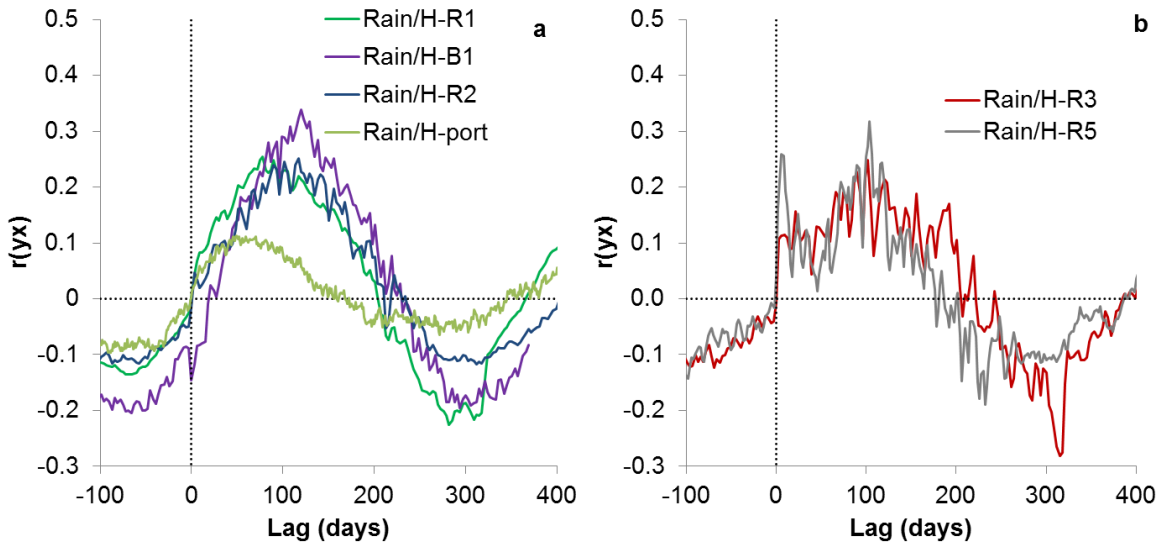

Figure 9: Cross-correlation between rainfall and water level (H) series deconvoluted from pumping effects using the MISO approach*: (a) B1, R1, R2 and Port wells, (b) R3 and R5 wells; r(yx): correlation coefficient; *except for Port well for which the cross-correlation is computed between rainfall and raw water levels data

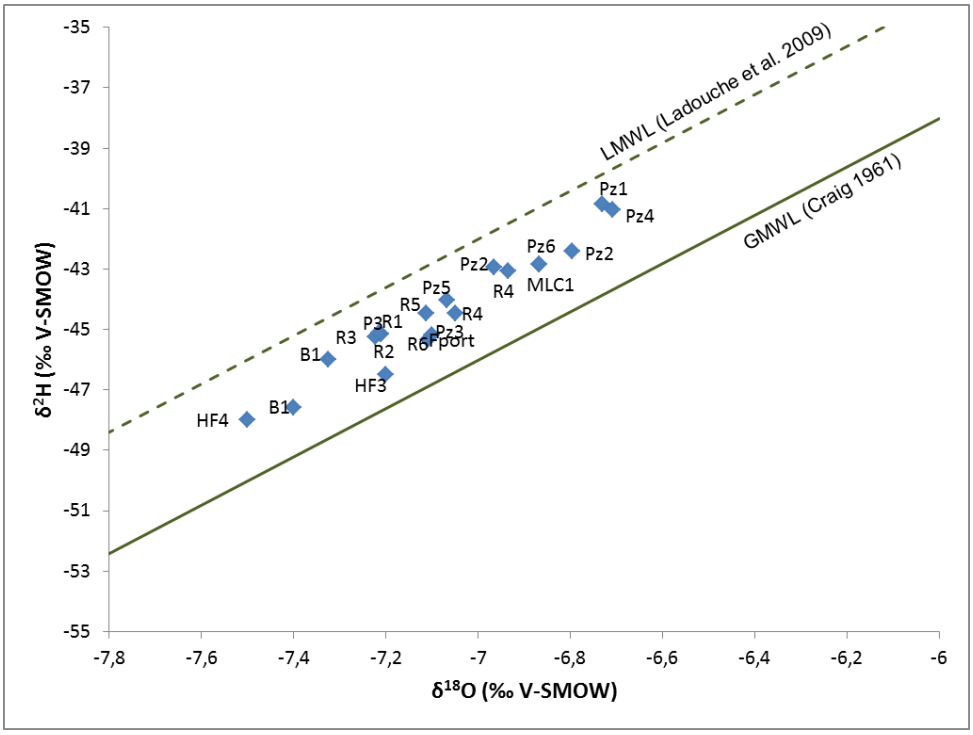

Figure 10 : Stable isotopes diagram (δ^2H vs$\delta^{18}O$) of La Salvetat groundwater; LMWL: local meteoric water line; GMWL: global meteoric water line

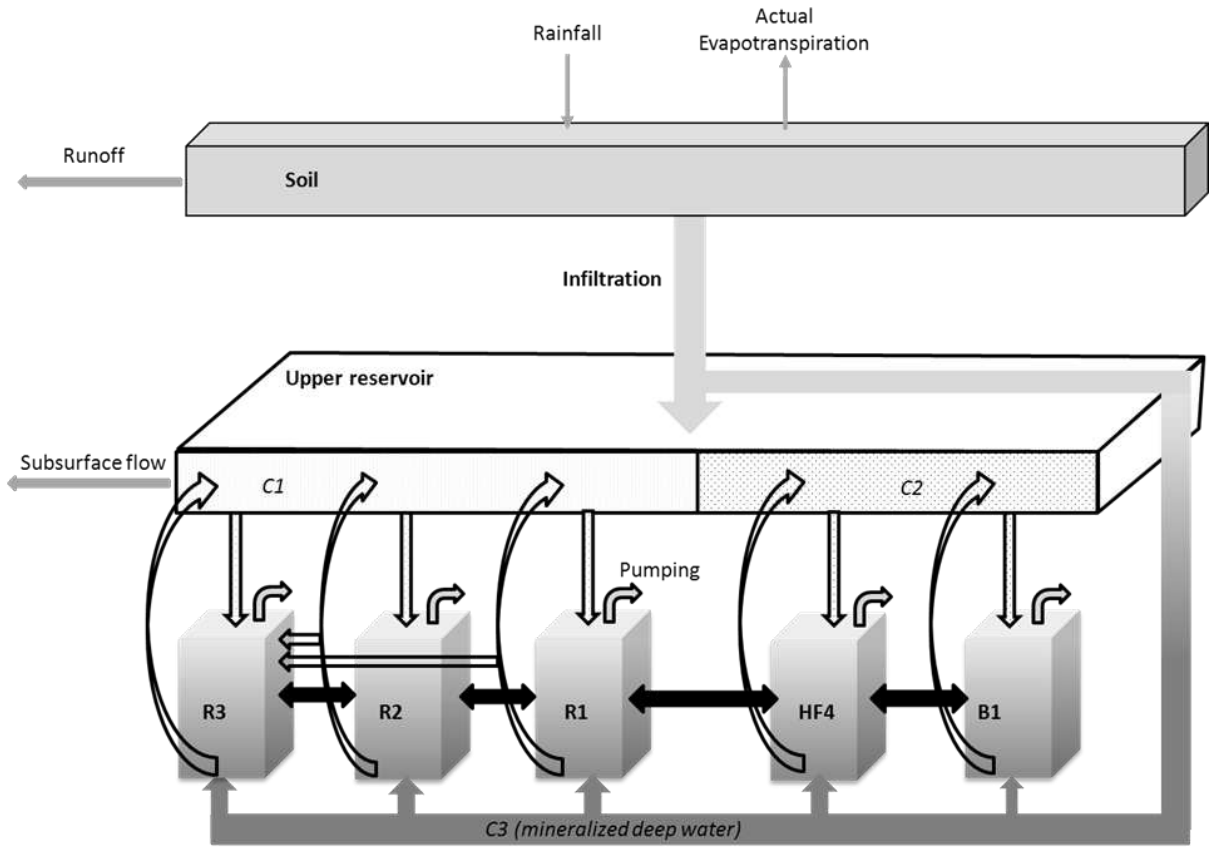

Figure 11: Conceptual flow diagram showing how the numerically modelled system functions (system B1-HF4-R1-R2-R3)

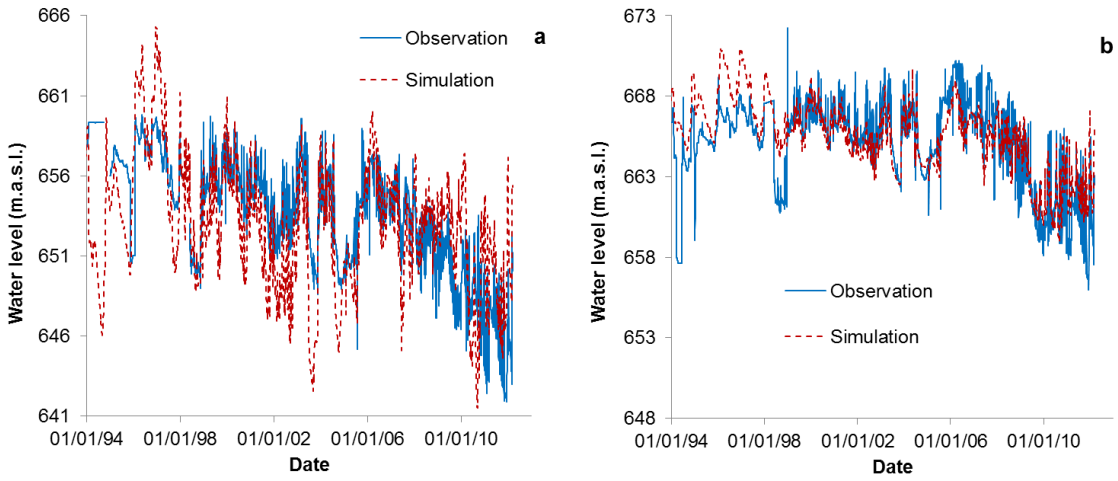

Figure 12: Comparison between observed piezometric levels corrected for quadratic head losses and simulated levels from 1991 to 2012 at wells (a) R1 and (b) R2

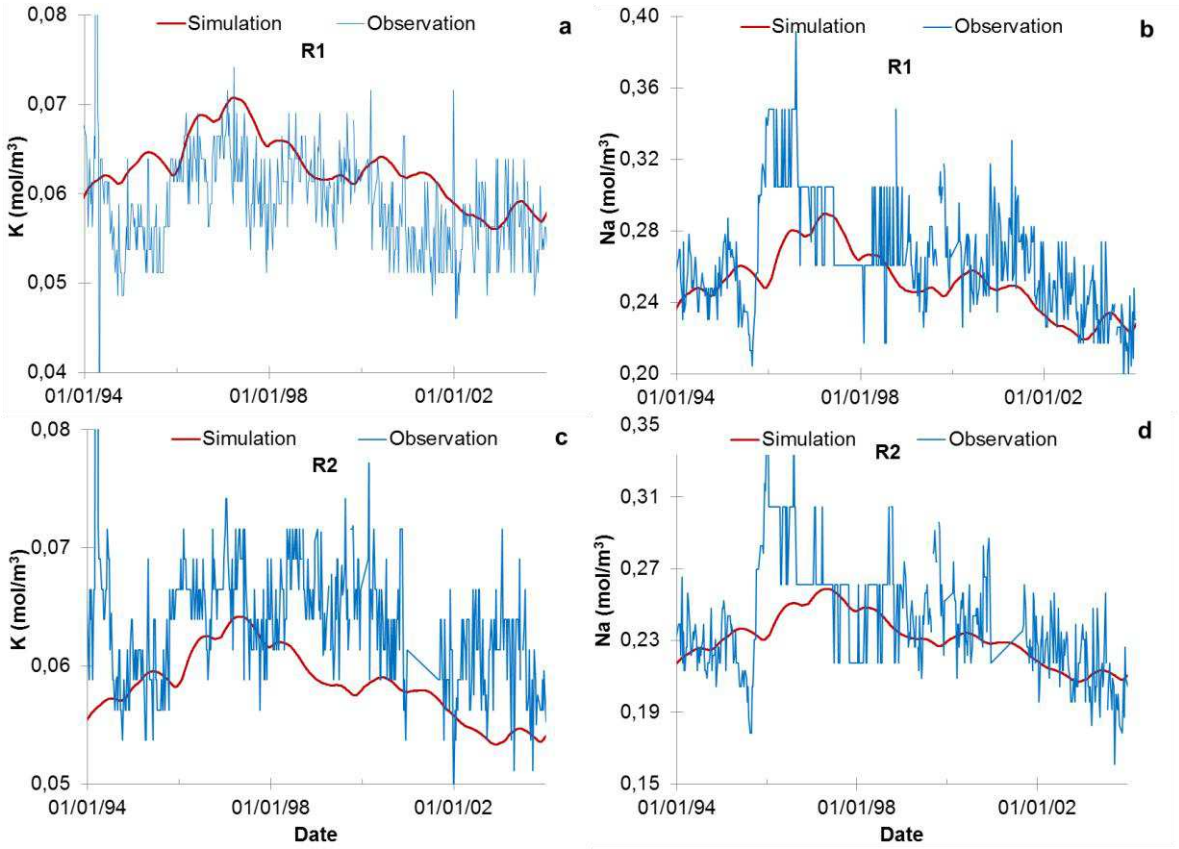

Figure 13: Concentrations observed and simulated at well R1 for (a) potassium and (b) sodium, and at well R2 for (c) potassiumand (d) sodium. The simulation period includes five successive rainy years (1992-1997) resulting in increased mineralisation of pumped water. This increase in concentration is well reproduced by the model.

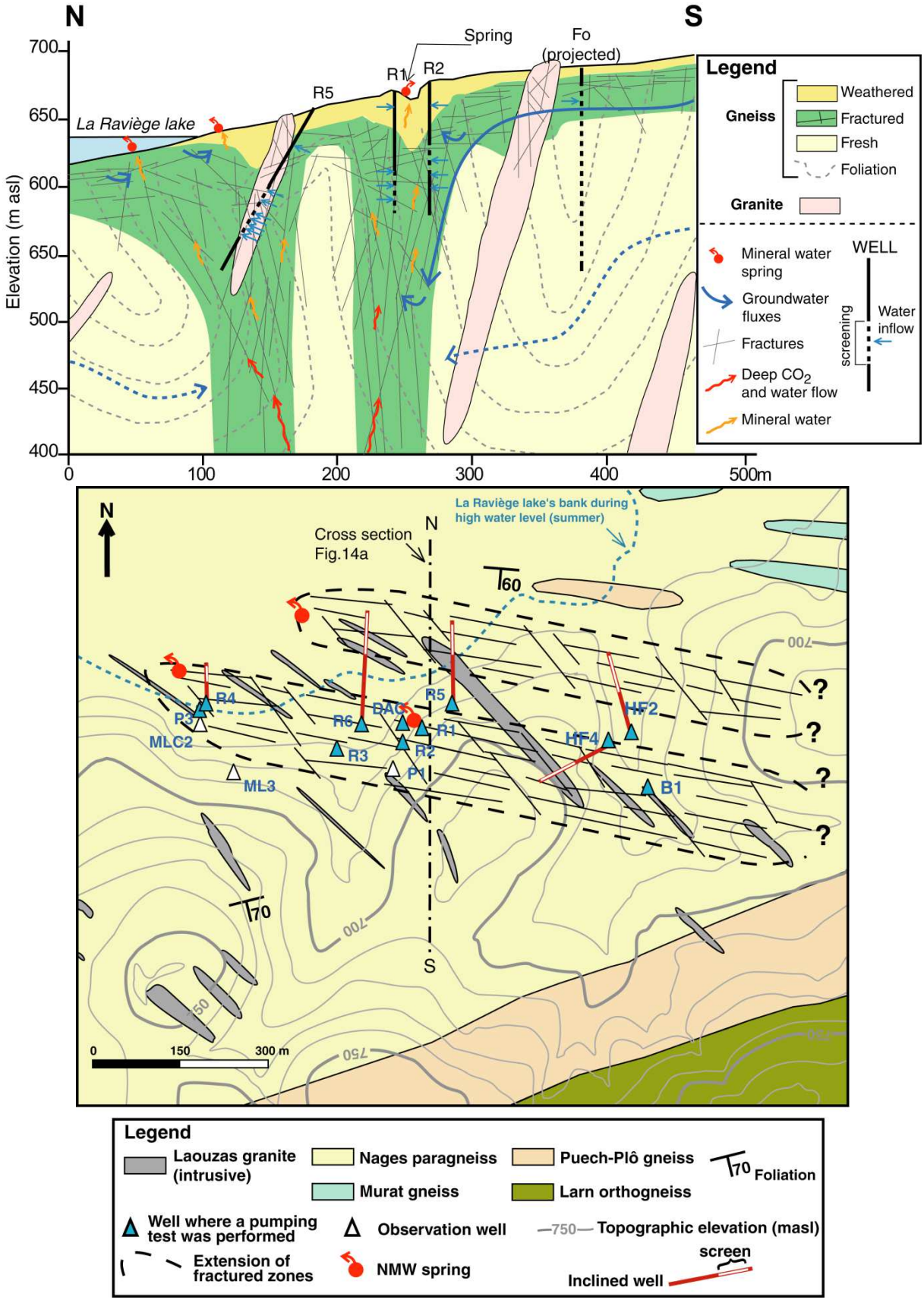

Figure 14: Conceptual hydrogeological model of the La Salvetat NMW reservoir (a) cross-cut view (b) plan view